Title : will be set by the publisher
Editors : will be set by the publisher
EAS Publications Series, Vol. ?, 2003

PULSARS

Michael Kramer[1]

Abstract. One of the most fundamental discoveries in physics and astrophysics was made with the discovery of pulsars. Ever since, pulsars – and later in particular binary and millisecond pulsars – have been studied as extreme end-states of stellar evolution, as super-dense objects, as radio and high-energy sources, as probes for the interstellar medium, and as super-precise clocks for fundamental experiments in gravitational physics. This article reviews some of the exciting applications of pulsar physics and the amazing prospects that are promised by the advent of the Square-Kilometre-Array (SKA).

1 Introduction

A new era in fundamental physics began when highly magnetized neutron stars were discovered as pulsars in 1967 (Hewish et al. 1968). In the following 35 years, these unique objects have been proven to be invaluable for the study of a wide variety of physical and astrophysical problems. Most notable are studies of gravitational physics, the interior of neutron stars, the structure of the Milky Way and stellar and binary evolution. Most, but not all, of these results have been obtained by pulsar timing. Other uses of pulsars depend on measuring their emission properties and/or the interaction of the radiation with an ambient medium. In the recent years, huge advances in observational high energy astrophysics have transformed pulsar astronomy to a true multi-wavelength science. In fact, pulsars are the only astrophysical sources that are observable in *every* astronomical window. These include not only all electromagnetic windows, but also that of gravitational wave astronomy which will be wide open as soon as the currently commissioned detectors reach their target sensitivities.

Clearly, the wealth of information that can be obtained outside the classical radio window today justifies some re-definition of the word "pulsar". Rather than being characterised by appearing as pulsating *radio* sources, a new definition of *pulsar* should be that it *emits radiation that is pulsed due to rotation and powered*

[1] University of Manchester, Jodrell Bank Observatory, Cheshire SK11 9DL, UK

© EDP Sciences 2003
DOI: (will be inserted later)

by rotational energy. This definition also encompasses X-ray pulsars that are clearly powered by the loss of rotational energy but which have not been detected at radio frequencies. This may be due to a misaligned radio beam or due to a very low radio luminosity. Nevertheless, it is fair to say that we still learn most about pulsars from high-sensitive radio observations. Because of this fact and in tribute to Karl Jansky and his work, we will concentrate on the radio aspect, but we will also cast views across the whole electromagnetic spectrum.

2 Pulsars as Neutron Stars

Pulsars are born in supernova explosions of massive stars. The most famous example is certainly the 33-ms Crab pulsar, PSR B0531+21 (Staelin & Reifenstein 1968), in the centre of the Crab Nebula which is the remnant of SN1054. Created in the collapse of the stars' core, neutron stars are the most compact objects next to black holes. From timing measurements of binary pulsars (see Section 8.1), we determine the masses of pulsars to be within a narrow range of $1.35 \pm 0.04 M_{\odot}$ (Thorsett & Chakrabarty 1999). Modern calculations for different equations of state produce results for the size of a neutron star quite similar to the very first calculations by Oppenheimer & Volkov (1939), i.e. about 20 km in diameter. Such sizes are consistent with independent estimates derived from modelling light-curves and luminosities of pulsars observed at X-rays (e.g. Zavlin & Pavlov 1998).

The structure of neutron stars is complex, with densities increasing from $\sim 10^6$ g cm^{-3} at the surface to $\sim 10^{15}$ g cm^{-3} at the centre. The outer layers consist of a solid rigid crust of crystalline structure, primarily of iron nuclei. Passing the density of the neutron drip point, the material becomes a super-liquid and superconducting mix of mainly neutrons but with some small proportion of protons and electrons (e.g. Link et al. 1999, Lattimer & Prakash 2001).

As rotating magnets, pulsars emit magnetic dipole radiation as the dominant effect for an increase in rotation period, P, described by $\dot{P}$. Equating the corresponding energy output of the dipole to the loss rate in rotational energy, we obtain an estimate for the magnetic field strength at the pulsar surface

$$B = 3.2 \times 10^{19} \sqrt{P\dot{P}} \text{ Gauss.} \tag{2.1}$$

Sometimes twice the value is quoted to reflect the field at the poles. Seemingly trivial, this point may become important when one studies the relationship between radio pulsars and the so-called "Magnetars". These are young, slowly-rotating neutron stars with periods ranging from $\sim$ 5 s to $\sim$ 12 s, observed as X-ray and Gamma-ray sources known as Soft-Gamma-Ray Repeaters (SGRs) and Anomalous X-ray Pulsars (AXPs) (see Kaspi 2004 for a recent review of these objects). Without a confirmed detection of magnetars at radio wavelengths (e.g. Lorimer & Xilouris 2000), the lack of radio emission has been attributed due to a magnetic field strength at the poles exceeding the quantum critical field, $B_{crit} = m_e^2 c^3 / e\bar{h} = 4.4 \times 10^{13}$ Gauss. Such a field strength could quench the

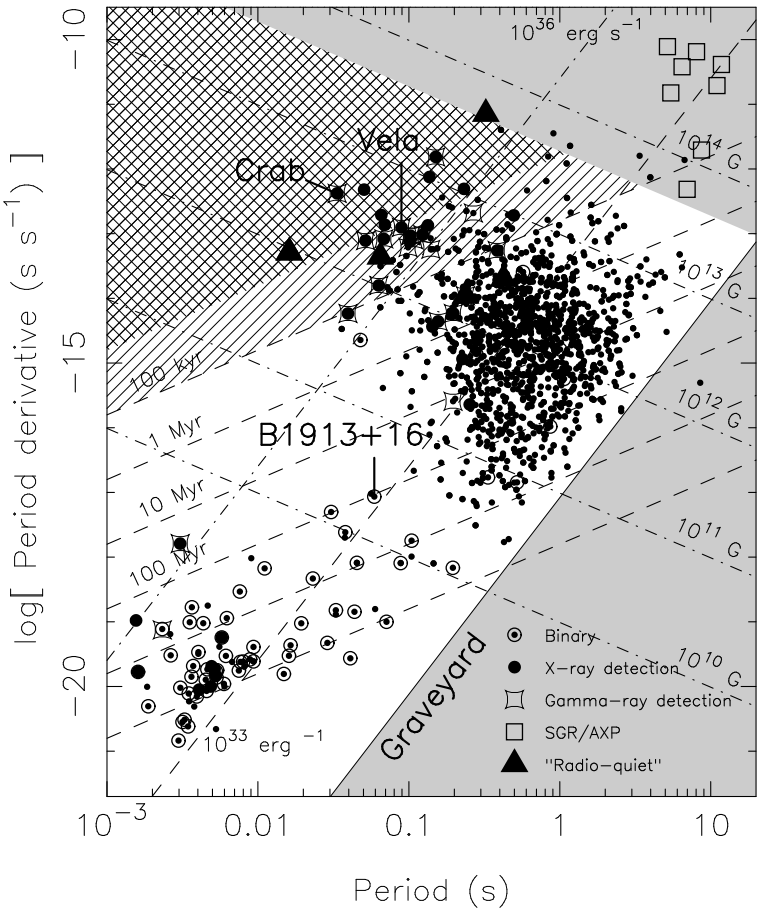

Fig. 1. $P - \dot{P}$–diagram of the currently known population of pulsars. The hatched area contains pulsars with spin-down ages of less than 100 kyr, whilst the cross-hatched area marks young pulsars with an age less than 10 kyr. Pulsars located in the upper grey area exhibit surface magnetic fields above the quantum critical field. Lines of constant spin-down luminosity of $\dot{E} = 10^{33}$ erg s^{-1} and $\dot{E} = 10^{36}$ erg s^{-1} are shown. Pulsars marked as large filled circles have been detected at X-ray frequencies, and pulsars with γ-ray detections are shown by sharply-edged squares. Normal squares indicate neutron stars identified as SGRs or AXPs. Spin-powered pulsars with not (yet?) visible as normal radio pulsars are shown as filled triangles. Binary pulsars are marked as circles filled with a dot.

creation of pair plasma that may be responsible for radio emission (e.g. Baring & Harding 1998, Zhang & Harding 2000). However, the discovery of pulsars with magnetar-like spin-parameters and derived magnetic fields well above the critical field, like the 6-s PSR J1847−0130 with $B \sim 10^{14}$ Gauss (McLaughlin et al. 2003),

questions the importance of the actual field value for the emission process.

For the majority of normal radio pulsars, we find magnetic field strengths of the order 10^{12} G. So-called millisecond pulsars have lower field strengths of the order of 10^8 to 10^{10} Gauss which appear to be a result of their evolutionary history (see Section 3). In general, these derived magnetic field strengths are consistent with values derived from X-ray spectra of neutron stars where we observe cyclotron lines (e.g. Bignami et al. 2003).

3 The Evolution & Population of Pulsars

As pulsars are powered by their rotational energy, their spin-frequency decreases. The slow-down can be described by

$$\dot{\nu} = -\text{const.}\ \nu^n \tag{3.1}$$

where the exponent, n, is known as the *braking index*. For magnetic dipole emission as the main energy loss, we expect $n = 3$. Measuring a second spin-frequency derivative, $\ddot{\nu}$, one can obviously determine the braking index via

$$n = \nu\ddot{\nu}/\dot{\nu}^2 \tag{3.2}$$

so that the assumption of dipole braking can be tested. However, this is only possible for the very youngest pulsars (Johnston & Galloway 1999), whilst rotational instabilities known as *timing noise* can mimic a significant but time-varying value of $\ddot{\nu}$. These values then reflect timing noise rather than regular spin-down, so that derived braking indices are meaningless (Hobbs et al. 2004). In total, only for five young pulsars could a braking index be determined that appears to reflect the long-term spin-down behaviour. With values ranging from $n = 1.4$ to $n = 2.9$ (e.g. Zhang et al. 2001), the deviations from the expected braking index are not too severe.

Integrating Eqn. 3.1, we can estimate the age of a pulsar from

$$\tau = \frac{P}{(n-1)\dot{P}} = \frac{P}{2\dot{P}} = -\frac{\nu}{2\dot{\nu}} \tag{3.3}$$

where we have assumed a magnetic dipole braking index of $n = 3$. This quantity known as the *characteristic age* is a valid estimate for the true age under the assumption that the initial spin period is much smaller than the present period. While it had been assumed in the past that pulsars are born with periods similar to that estimated for the Crab pulsar, $P_0 = 19$ ms (Lyne et al. 1993), recent estimates suggest a wide range of initial spin periods from 14 ms up to 140 ms (Kramer et al. 2003c).

We can describe the evolution of a pulsar in period, P, and slow-down, $\dot{P}$, in a logarithmic P-$\dot{P}$-diagram as shown in Figure 1 where we plot all of the $\sim$ 1700 pulsars currently known for which P and $\dot{P}$ have been measured. Since the estimates for both magnetic field (Eqn. 2.1) and characteristic age (Eqn 3.3)

depend only P and $\dot{P}$, we can draw lines of constant magnetic field and constant characteristic age. Accordingly, young pulsars should be located in the upper left area of Fig. 1. Pulsars are generally considered to be young if their characteristic age is less than 100 kyr. Specifically, pulsars with characteristic ages of less than 10 kyr appear in the cross-hatched area, whilst pulsars with ages between 10 and 100 kyr are located in the hatched area. The latter pulsars are often compared to the Vela pulsar if they match its *spin-down luminosity*, i.e. $\dot{E} \gtrsim 10^{36}$ erg s^{-1}. The spin-down luminosity is simply given by the loss in rotational energy which can be measured from the observed period and period derivative,

$$\dot{E} = 4\pi^2 I \dot{P} P^{-3} \text{ erg s}^{-1} \tag{3.4}$$

where a neutron star moment of inertia of $I = 10^{45}$ g cm^2 is assumed. Obviously, $\dot{E}$ represents the maximum energy output available for spin-powered pulsars across the *whole* electromagnetic spectrum. As we will see, the radio output is tiny compared to that at high energies.

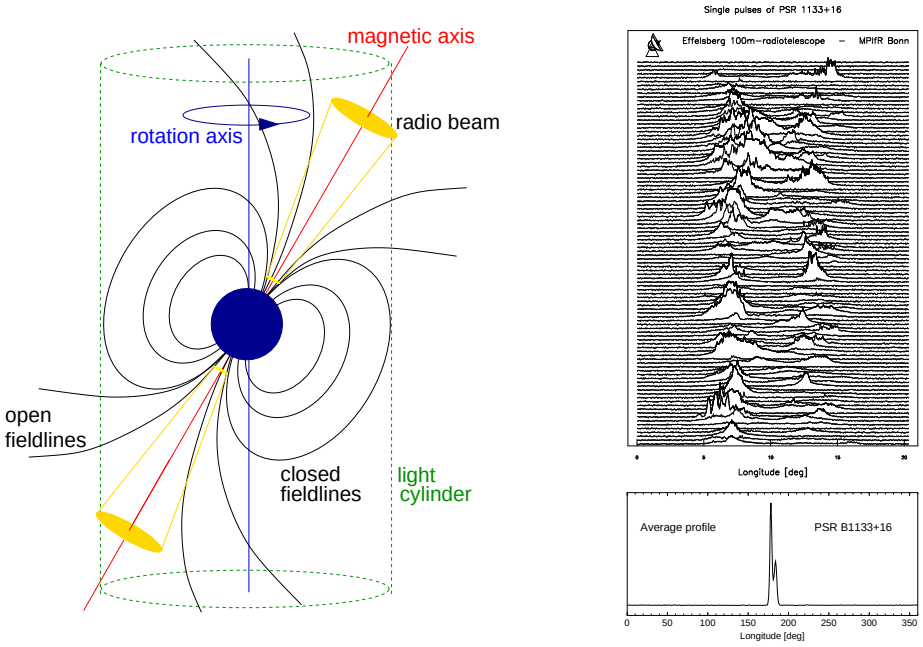

Fig. 2. *Left:* A pulsar is a rotating, highly magnetised neutron star. A radio beam centred on the magnetic axis is created at some height above the surface. The tilt between the rotation and magnetic axes makes the pulsar in effect a cosmic lighthouse when the beam sweeps around in space. *Right:* Individual pulses vary in shapes and strength (top), average profiles are stable (bottom). The typical pulse width is only ∼4% of the period.

A line of a constant, Vela-like $\dot{E} = 10^{36}$ erg s^{-1} is shown in Fig. 1 together

with a line for $\dot{E} = 10^{33}$ erg s^{-1}. About 26 Vela-like pulsars are currently known (Kramer et al. 2003a). In comparison, there are only 6 Crab-like pulsars, including the fastest rotating young but radio-quiet pulsar PSR J0537−6910 with a period of only 16 ms (Marshall et al. 1998). In the same group we also find PSR J1119−6137 with the youngest age and highest $\dot{P}$ for any known radio pulsar. The overall records are currently set by the radio-quiet PSR J1846−0258 in Kes75 with a period of 323 ms and a characteristic age of only 722 yr (Gotthelf et al. 2000).

When pulsars age, they move into the central part of the $P-\dot{P}$-diagram where they spend most of their lifetime. Consequently, most known pulsars have spin periods between 0.1 and 1.0 s with period derivatives of typically $\dot{P} = 10^{-15}$ s s^{-1}. Selection effects are only partly responsible for the limited number of pulsars known with very long periods, the longest known period being 8.5 s (Young et al. 1999). The dominant effect is due to the "death" of pulsars when their slow-down has reached a critical state. This state seems to depend on a combination of P and $\dot{P}$ which can be represented in the $P-\dot{P}$-diagram as a *pulsar death-line*. To the right and below this line (see Figure 1) the electric potential above the polar cap may not be sufficient to produce the particle plasma that is responsible for the observed radio emission. While this model can indeed explain the lack of pulsars beyond the death-line, the truth may be more complicated as the position of the 8.5-sec pulsar deep in the *pulsar graveyard* indicates. Nevertheless, it is clear that the normal life of radio pulsars is limited and that they die eventually after tens to a hundred million years.

The position of a sub-set of about 100 pulsars located in the lower left part of Fig. 1 cannot be explained by the above picture of normal pulsar life. Instead, these pulsars simultaneously have small periods (of the order of milliseconds) and small period derivatives, $\dot{P} \lesssim 10^{-18}$ s s^{-1}. They appear much older than ordinary pulsars (see Eqn. 3.3) and, indeed, these so-called *millisecond pulsars* represent the oldest population of pulsars with ages up to $\sim 10^{10}$ yr. A model for their evolutionary history was proposed soon after the discovery of PSR B1937+21 by Backer et al. in 1982. This first millisecond pulsar has a period of only 1.56 ms and remains the pulsar with the shortest period known.

It is suggested that millisecond periods are obtained when mass and thereby angular momentum is transferred from an evolving binary companion while it overflows its Roche lobe (e.g. Alpar et al. 1982). In this model, millisecond pulsars are recycled from a dead binary pulsar via an X-ray binary phase. This model implies a number of observational consequences: a) most normal pulsars do not develop into a millisecond pulsar as they have long lost a possible companion during their violent birth event; b) for surviving binary systems, X-ray binary pulsars represent the progenitor systems for millisecond pulsars; c) the final spin period of recycled pulsars depends on the mass of the binary companion. A more massive companion evolves faster, limiting the duration of the accretion process; d) the majority of millisecond pulsars have low-mass white-dwarf companions as the remnant of the binary star. These systems evolve from low-mass X-ray binary systems (LMXBs); e) high-mass X-ray binary systems (HMXBs) represent the progenitors for double neutron star systems (DNSs). DNSs are rare since these

systems need to survive a second supernova explosion. The resulting millisecond pulsar is only mildly recycled with a period of tens of millisecond.

The properties of millisecond pulsars and X-ray binaries are consistent with the described picture. For instance, it is striking that $\sim 90\%$ of all millisecond pulsars are in a binary orbit while this is true for only less than 1% of the non-recycled population. For millisecond pulsars with a low-mass white dwarf companion the orbit is nearly circular, although the details depend on the exact nature of the companion star and the initial orbit. In case of double neutron star systems, the orbit is affected by the unpredictable nature of the kick imparted onto the newly born neutron star in the asymmetric supernova explosion of the companion. If the system survives, the result is typically an eccentric orbit with an orbital period of a few hours.

4 Pulsars as Radio Sources

Pulsars are highly magnetized, rotating neutron stars which emit a narrow radio beam along the magnetic dipole axis. As the magnetic axis is inclined to the rotation axis, the pulsar acts like a cosmic light-house emitting a radio pulse that can be detected once per rotation period when the beam is directed towards Earth (Figure 2). The radio signal of a pulsar is usually weak, both because the pulsar is distant and the size of the actual emission region is small. Estimates range down to a few metres, resulting in brightness temperatures of up to 10^{37} K (Hankins et al. 2003). Such values require a coherent emission mechanism which, despite 35 years of intensive research, is still unidentified. However, we seem to have some basic understanding, in which the magnetized rotating neutron star induces an electric quadrupole field which is strong enough to pull out charges from the stellar surface (the electrical force exceeds the gravitational force by a factor of $\sim 10^{12}$!). The magnetic field forces the resulting dense plasma to co-rotate with the pulsar. This *magnetosphere* can only extend up to a distance where the co-rotation velocity reaches the speed of light[1]. This distance defines the so-called light cylinder which separates the magnetic field lines into two distinct groups, i.e. *open and closed field lines*. The plasma on the closed field lines is trapped and co-rotates with the pulsar forever. In contrast, plasma on the open field lines can reach highly relativistic velocities and can leave the magnetosphere, creating the observed radio beam at a distance of a few tens to hundreds of km above the pulsar surface (e.g. Kramer et al. 1997, see Fig. 2).

Individual radio pulses provide a "snapshot" of the plasma processes occurring in the pulsar magnetosphere at an instant, resulting in varying, often seemingly random looking pulses (see Fig. 2). Unfortunately, only a limited number of pulsars are strong enough to enable single pulse studies. These nevertheless promise to be the best way to investigate plasma creating processes (e.g. Deshpande &

[1] Strictly speaking, the Alfvén velocity will determine the co-rotational properties of the magnetosphere.

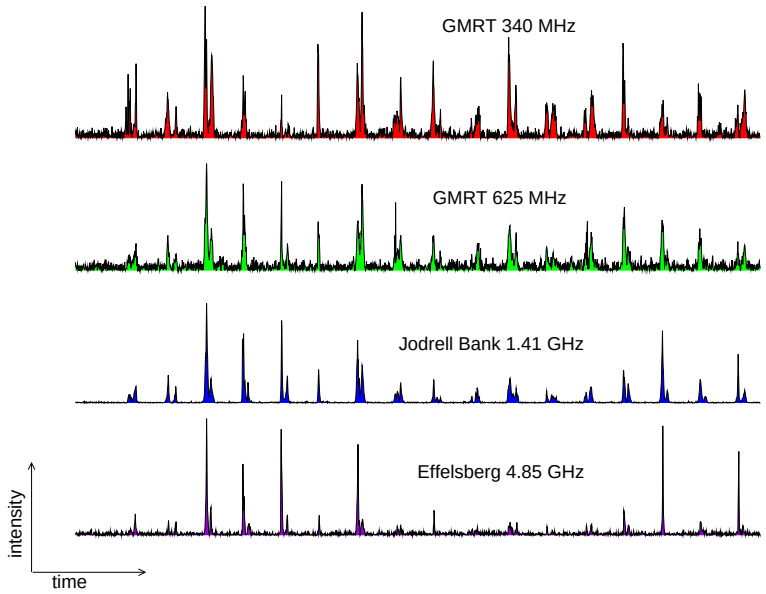

Fig. 3. Single pulses of PSR B1133+16 simultaneously observed with three different telescopes at four different frequencies (Karastergiou et al. 2004).

Rankin 2001) and emission properties and hence the radiation process. The comparison of data obtained at several frequencies at the same time offers the possibility of distinguishing between propagation effects and of properties inherited from the original radiation process. This has been demonstrated recently in a series of papers by Karastergiou et al. (2001, 2002, 2003). Since simultaneous multi-frequency observations are difficult to realize with a single telescope, coordinated multi-station experiments are necessary. An example of such experiment is given in Figure 3.

All information about dynamical processes in the pulsar magnetosphere is lost if only an integrated pulse shape, the *pulse profile*, can be observed. The average pulse profile reflects the global constraints given by geometrical factors and a conal beam structure with, possibly, a beam pattern. Apart from a frequency dependence, the profile is stable and independent of the particular pulses added (see Fig. 2). It is this profile stability which allows us to time pulsars to high precision.

Usually, pulsar emission is also highly elliptically polarized, up to 100%. Separating the polarized emission into linearly and circularly polarized components, the linear component is by far dominant (see Fig. 4). Pulsars with up to 30% circular polarization or more are nevertheless not uncommon. The degree of polarisation decreases with increasing frequency (e.g. Xilouris et al. 1996). Polarisation serves as a useful diagnostic tool, both to probe the pulsar magnetosphere

(e.g. Karastergiou et al. 2000) and to obtain information about the viewing geometry (Radhakrishnan & Cooke 1969, see Fig. 4).

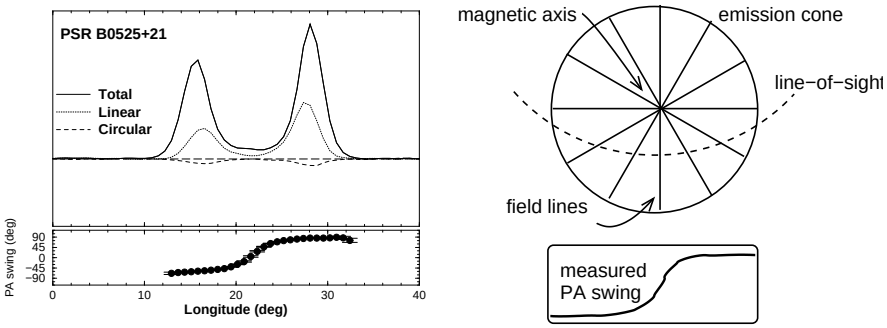

Fig. 4. *Left:* Polarization profile of PSR B0525+21. The elliptically polarized emission has been split into a linearly and circularly polarized component. The position angle (PA) of the linear component shows the typical S-like swing that can be understood geometrically in terms of a rotating-vector model (RVM). *Right:* The RVM by Radhakrishnan & Cooke (1969) explains the PA-swing by the projection of the magnetic field line direction onto our line-of-sight cutting the emission cone.

The median luminosity observed at 1400 MHz is $L_{1400} = 4 \pm 1$ mJy kpc^2 (Kramer 2004b). There is a slight trend for older pulsars to be less luminous but this is mostly suggested by the millisecond pulsars which are indeed less luminous and less efficient radio emitters (Kramer et al. 1998). The flux density spectrum, $S \propto \nu^{\alpha}$, is steep with a mean spectral index of $\alpha \sim -1.7$. No age dependence is found despite earlier reports to the contrary (Maron et al. 2000). The highest radio frequency that pulsars have been detected at is 87 GHz (Morris et al. 1997), and there are indications for a spectral turn-up at mm-wavelengths (Kramer et al. 1996). These observations at very high frequencies are interesting due to a suggested *radius-to-frequency mapping* (RFM), according to which high frequency radio emission originates from closer to the neutron star surface than low frequency emission (Cordes 1978). The model is motivated by the observation that pulse profiles become narrower at high frequencies. However, it seems difficult to decide whether the derived magnetospheric altitudes correspond to the heights where the emission is *created* or where it *escapes* the magnetosphere after it had been created further down and propagated to the escape radius, possibly in certain wave modes. In any case, there seems to be no doubt that the classical radio emission originates from a few hundred km or so above the pulsar surface, and that the radiating plasma originates from the polar cap region. The interesting question is thereby how this plasma is related to that creating high energy emission, for which competing models place the origin near the polar cap as well (e.g. Daugherty & Harding 1996) or further out in the magnetosphere in so-called "outer gaps" (e.g. Cheng et al. 1986). Clues are available from radio *giant pulses* observed for a handful of pulsars which we will discuss in Section 6.

5 Pulsars as High Energy Sources

While the majority of spin-powered pulsars are still discovered and studied at radio frequencies, an increasing number can be observed at high energies. Particularly, a handful of pulsars are only visible as pulsating X-ray sources, so that they appear to be "radio-quiet". These are marked in the $P - \dot{P}$–diagram presented in Figure 1. The energy output of spin-powered pulsars is largest at high energies. This becomes clear when comparing the luminosities at corresponding frequency bands with the spin-down luminosity, $\dot{E}$. Detailed comparisons are difficult to due different beaming fractions, but a general trend is visible as $\eta_\nu = L_\nu/\dot{E} \propto \nu^{0.17\pm0.10}$ (see Fig. 5, Kramer 2004b).

5.1 Optical Frequencies

Currently, only five pulsars are reported to show pulsed optical emission (see e.g. Shearer & Golden 2002 for a review). The prime example is the Crab pulsar which is strong enough to allow extensive studies of its single pulses and their polarization properties (e.g. Romani et al. 2001, Kanbach et al. 2003). A striking similarity between the optical, X-ray and gamma-ray profiles suggests that the emission is created by the same incoherent non-thermal radiation process, presumably at the same location. The polarization measurements and the applications of the rotating-vector model thereby enable studies of the geometry of the corresponding emission region in a way that is not yet possible at X-rays. Such studies are not possible for the other weaker pulsars with detected pulsed emission, i.e. Vela, Geminga and PSRs B0656+14 and B0540−69. Unpulsed emission has been detected for four pulsars, including PSR B1055−52 which together with the Crab, Vela, Geminga and possibly PSR B0656+14 is also detected as a gamma-ray pulsar (e.g. Thompson 2001), again suggesting that the optical emission is closely related to the X-ray and gamma-ray emission.

5.2 X-ray Frequencies

X-ray observations promise to offer a more direct insight into the magnetospheric plasma densities and processes when compared to the view provided by radio observations that is somewhat occluded by the (unknown) physics responsible for the coherence of the radio emission. However, in many pulsars the observed X-ray emission is due to a mixture of thermal and non-thermal processes which cannot always be discriminated by the available data. Non-thermal, magnetospheric emission can be created by an accelerated relativistic plasma and should be highly pulsed with a power-law spectrum ranging from optical to gamma-ray frequencies. Thermal emission may originate from the stellar surface and may still show low-amplitude modulation due to the rotating hot polar cap. In this case, we would expect a blackbody spectrum that is modified by a possible atmosphere of the neutron star, ranging from optical to soft X-ray frequencies. In addition, matters may be complicated due to unresolved emission from pulsar-driven synchrotron

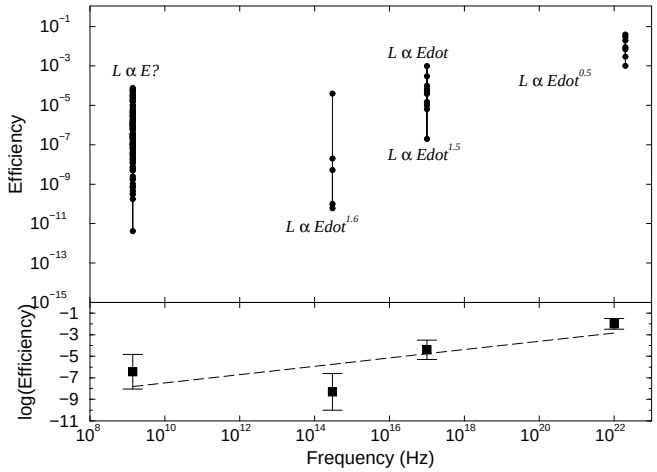

Fig. 5. Efficiency, $\eta \equiv L_\nu/\dot{E}$, as derived for radio, optical, X-ray and γ-ray frequencies. A fit to the median values shows an increase of efficiency with frequency of $\eta \propto \nu^{0.17\pm0.10}$. See Kramer (2004b) for details.

nebulae or pulsar winds interacting with dense ambient media. Pulsed emission has been observed for 15 normal radio pulsars and 6 millisecond pulsars (Fig. 1). In addition, 9 normal pulsars and 17 millisecond pulsars have only been seen as unpulsed X-ray sources (see Becker & Aschenbach 2002 for a review). In addition, Geminga and PSRs J0537−6910, J1209−51/52, J1811−1925 and J1846−0258 are clearly spin-powered pulsars at X-rays but have no corresponding radio detection, yet. In general, it is instructive to group the X-ray detected normal pulsars into Crab-like sources, Vela-like sources and middle-aged pulsars. The Crab-like pulsars show strong features of magnetospheric emission and doubled-peaked profiles which are, if detected, aligned with similar optical profiles. For Vela-like pulsars only Vela itself has been detected as a faint optical source. Their X-ray spectra do not represent simple power-laws whilst the pulse profiles are more complicated and typically misaligned with radio or gamma-ray pulses. Finally, the middle-aged pulsars show a mixture of thermal and non-thermal emission with energy-dependent profiles.

5.3 Gamma-ray Frequencies

The gamma-ray emission of pulsars is highly pulsed, beamed and, obviously, of non-thermal origin. There are 7 "classical" gamma-ray detections, i.e. Crab, Vela, Geminga and PSRs B1055+53, B1509−58, B1706−44 and B1951+32 (see e.g. Thompson 2001 or Kanbach 2002 for recent reviews). Their typically double-peaked profiles change their appearances towards higher energies due to a phase-dependent spectral hardness, suggesting that, like in the radio, geometry plays an important role. Similar studies are not possible for other, much weaker pulsars for

which a detection has been suggested. Here, significance levels are much lower, and often their detection is based on the positional coincidence of a known radio pulsar with an unidentified gamma-ray point source. A viable pulsar candidate should have properties consistent with those of the classical gamma-ray pulsars, shown to be steady gamma-ray sources (e.g. McLaughlin et al. 1996). While the beaming fraction is uncertain, the γ-ray luminosity seems to be a few per cent of the spin-down luminosity (Kramer et al. 2003a). Ultimately, it will need instruments like GLAST to verify most of these candidates. By extending the observed γ-ray spectrum to a few tens GeV, GLAST may then also be able to distinguish between the outer gap and polar cap model. The polar cap model interprets the observed emission as inverse Compton scattering of upward polar cap cascades and expects a cut-off of the spectrum due to γ-B-field absorption. In contrast, the spectrum expected for the outer gap particles is curvature radiation limited and should extend to higher energies (e.g. Thompson 2001).

6 Giant Pulses or The Radio–High-Energy Connection

The phenomenon of giant radio pulses has been detected and studied in the Crab pulsar (e.g. Sallmen et al. 1999), PSR B0540−69 (Johnston & Romani 2003), and the millisecond pulsars B1937+21 (e.g. Backer 1995, Cognard et al. 1996), B1821−24 (Romani & Johnston 2001) and J0218+4232 (Joshi et al. 2004). The working definition of giant pulses is a flux density in a single pulse which is more than 10 times the mean flux density. Whilst in the vast majority of pulsars, very few – if any – single pulse fluxes exceed 10 times the mean flux density, pulsars with giant pulses show occasional pulses in excess of 1000 times the mean pulsed flux. Interestingly, this peculiar sample of pulsars with giant pulse emission includes both very young as well as very old pulsars. However, all these pulsars are also detected at high energies. Another common feature these pulsars share is the highest (estimated) magnetic field at their light cylinders (cf. Cognard et al. 1996, see Fig. 6). It is unclear whether this is related to the physics of giant pulses but it is interesting that this property of the outer magnetosphere may connect the giant pulse radio emission to the place of origin that is suggested for high-energy emission. Indeed, the giant pulses often occur misplaced from the normal radio profile but appear to be aligned with X-ray and/or Gamma-ray emission (see Romani & Johnston 2001, Fig. 6). This suggests a common origin, indicating that some observed radio emission could be in fact a by-product of the high energy radiation process. This could explain the highly unusual "High-Frequency Components", seen to emerge at some odd pulse phases in the Crab profile at a few GHz (Moffett & Hankins 1996), as the results of such possible by-products and geometrical RFM-like effects. A related phenomenon may also be the recently discovered *giant micropulses* (Johnston et al. 2001) which have been found for the Vela pulsar and PSR B1706−44. These pulses are very narrow ($\sim 100\mu$s) (i.e. still much wider than the nanosecond fine-structure seen by Hankins et al. (2003) in the Crab giant pulses), and exceed often 100× the expected flux density *at those pulse phases*. However, they have only rather little effect on the

pulse integrated flux density due to their narrow width. But again, both pulsars tend to have much higher magnetic field at the light cylinder than the average pulsar and both pulsars are high energy sources (see Fig. 6).

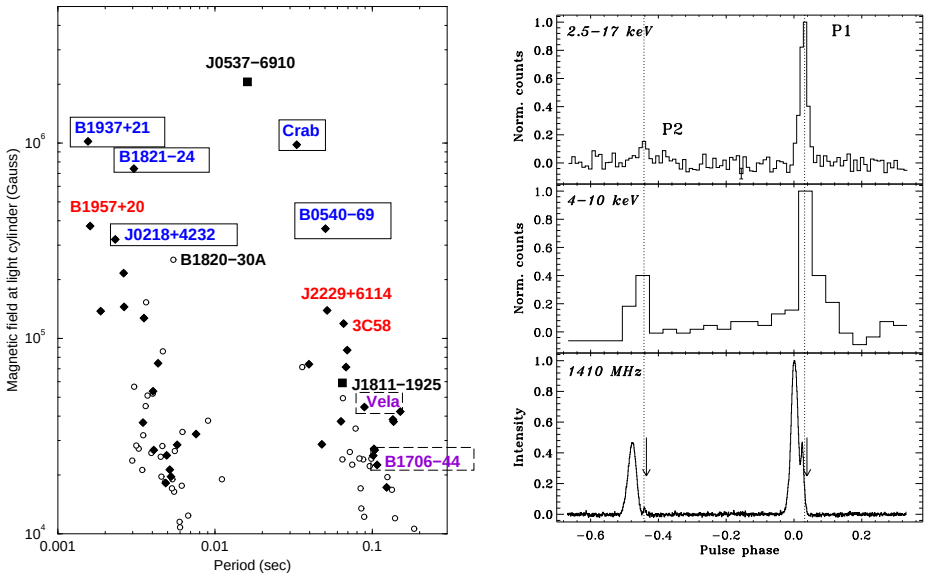

Fig. 6. *Left:* Magnetic field strength at the light cylinder. Filled diamonds mark pulsars detected both at radio and high-energies. Radio-quiet pulsars are shown as filled squares. Pulsars with detected giant pulse emission are surrounded by a box. The Vela pulsar and PSR B1706−44 show so-called "micro-giants" (see text). *Right:* RXTE pulse profile of PSR B1937+21 in the 2–17 keV energy band as presented by Cusumano et al. (2003, top) with the 4–10 keV BeppoSAX profile (Nicastro et al. 2003, middle) and a radio pulse profile obtained at 1.6 at Effelsberg (Kramer et al. 1998). Vertical arrows indicate the phases of observed radio giant pulses (see Cusumano et al. 2003 for details).

Giant pulses may finally provide the clue to connect the emission across the whole electromagnetic spectrum. Indeed, there also appears to be a direct observational link between the radio giant pulses of the Crab and its optical emission (Shearer et al. 2003). Therefore, a picture emerges in which the radio emission originates from close to the stellar surface, while the high energy emission may tend to be created further out. Consequently, one would not expect an alignment of radio and high-energy profiles, as typically observed. Where alignment is observed, like for the Crab pulsar, the observed radio emission may be of different origin and more related to that at high energies. Only the Crab's pre-cursor component may be considered as the classical radio pulse, while main and interpulse are by-products of high energy processes causing also the High-Frequency Components at a few GHz. If that is the case, the Crab pulsar should be considered as a much less luminous radio source, similar to PSR B0540−69 when ignoring its

giant pulse emission (Johnston & Romani 2003).

7 Pulsar Timing

By measuring the arrival time of the pulsar signals very precisely, we can study effects that determine the propagation of the pulses in four-dimensional space-time. Millisecond pulsars are the most useful objects for these investigations: their pulse arrival times can be measured much more accurately than for normal pulsars (the measurement precision scales essentially with spin frequency) and their rotation is much smoother, making them intrinsically better clocks.

The spin frequency of a pulsar can be expressed in a Taylor expansion,

$$\nu(t) = \nu_0 + \dot{\nu}(t - t_0) + \frac{1}{2}\ddot{\nu}(t - t_0)^2 + ... \tag{7.1}$$

where ν_0 is the spin frequency at reference time t_0, i.e. $\nu_0 = \nu(t_0) = 1/P_0$ with P_0 being the corresponding pulse period. While ν_0 is referring to a certain epoch, the parameters $\dot{\nu}$, $\ddot{\nu}$ are determined by the physical process responsible for the pulsar slow-down and should be constant for most time-spans considered (see Section 3, Eqn. 3.1).

Since the observing frame is not inertial, as we are using telescopes that are located on a rotating Earth orbiting the Sun, we need to transfer the times-of-arrival (TOAs) measured at the observatory to the centre of mass of the solar system (SSB) as the best approximation to an inertial frame available. The transformation of an observed topocentric TOA to a barycentric arrival time, $t_{\rm SSB}$, is given by

$$\begin{aligned} t_{\rm SSB} = \quad & t_{\rm topo} - t_0 + t_{\rm corr} - D/f^2 \ , & (7.2)\\ + \quad & \Delta_{\rm Roemer,\odot} + \Delta_{\rm Shapiro,\odot} + \Delta_{\rm Einstein,\odot} \ , & (7.3)\\ + \quad & \Delta_{\rm Roemer,Bin} + \Delta_{\rm Shapiro,Bin} + \Delta_{\rm Einstein,Bin} & (7.4) \end{aligned}$$

We have split the transformation into three lines. The first two lines apply to every pulsar whilst the third line is only applicable to binary pulsars.

The first line includes clock corrections applied retroactively to transform the measured time to a time standard such as UTC of BIPM. Further corrections take into account that the Earth is not rotating uniformly, modifying the effective arrival time at the telescope. As the pulses are delayed due to dispersion in the interstellar medium, the arrival time depends on the observing frequency, f. The TOA is therefore corrected for a pulse arrival at an infinitely high frequency.

The second line corrects for propagation in the solar system. The *Roemer delay*, $\Delta_{\rm Roemer,\odot}$, corrects for (classical) light-travel time from the telescope to SSB. The *Shapiro delay*, $\Delta_{\rm Shapiro,\odot}$, is a relativistic term that corrects for an extra delay due to the curvature of space-time in the solar system (Shaprio 1964). The last term in the second line, $\Delta_{\rm Einstein,\odot}$, is called *Einstein delay* and it describes the combined effect of gravitational redshift and time dilation due to motion of the Earth and other bodies, taking into account the variation of an atomic clock on Earth in the

varying gravitational potential as it follows its elliptical orbit around the Sun. The third line contains corresponding terms for pulsars in a binary system.

Equation 7.2-7.4 is sufficient to measure the clock rate as produced by the pulsar if no further motion or acceleration between pulsar and SSB occurs. If the pulsar is moving relative to the SSB, only the transverse component of the velocity, v_t, can be observed. A radial motion is not measurable, unless the pulsar has an optically detectable companion such as a white dwarf for which Doppler shifts can be measured from optical spectra. Otherwise, the effects of any radial velocity are absorbed in Doppler corrections to the observed periods and cannot be determined. In contrast, the transverse motion will add a linear time-dependent term and can therefore be measured as proper motion, μ. A proper motion will also affect measured quantities due to a "secular acceleration", known as the *Shlovskii Effect*, and/or changes in the geometrical orientation of a binary system. Finally, for a number of millisecond pulsars a *timing parallax* can be measured. In comparison to the more familiar positional parallax, it corresponds to measuring the time delay due to the curvature of the emitted wavefronts at different positions of the Earth orbit.

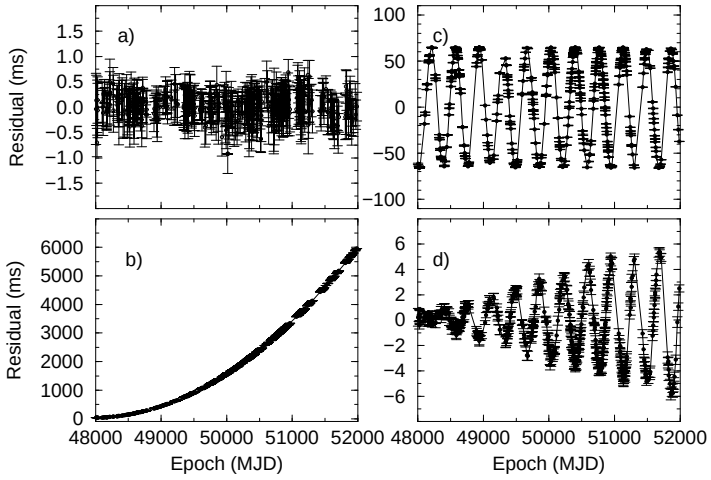

Fig. 7. Timing residuals for the 1.19-s pulsar B1133+16. A fit of a perfect timing model should result in randomly distributed residuals, shown in a). A parabolic increase in the residuals in part b) is obtained if $\dot{P}$ is underestimated, here by 4%. An offset in position produces sinusoid residuals shown in part c) where the declination has an error of 1 arcmin. Part d) demonstrates the effect of neglected proper motion, here of $\mu = 380$ mas/yr. Note the different scales on the y-axes.

Most of the parameters in Eqn. 7.2-7.4 are not known *a priori* (or only with limited precision after the discovery of a pulsar) and need to be determined precisely in a least-squares fit analysis of the measured TOAs. These parameters can be categorised into three groups:

Astrometric parameters: The astrometric parameters include the position of the pulsar, and its proper motion and parallax. While the position is only known within a telescope beam after the discovery, the precision can be greatly improved by timing the pulsar for about a year (full Earth orbit). Proper motion and parallax only become evident after a longer time-span.

Spin parameters: These include the rotation frequency of the pulsar, ν, and its derivatives (Eqn. 7.1).

Binary parameters: For pulsars in a binary orbit, the initial observations will typically show a periodic variation in observed pulse period. Five Keplerian parameters then need to be determined: orbital period, P_b; the projected semi-major axis of the orbit, $x \equiv a \sin i$ where i is the (usually unknown) inclination angle of the orbit; the orbital eccentricity, e; the longitude of periastron, ω; and the time of periastron passage, T_0. For a number of binary systems this Newtonian description of the orbit is not sufficient and relativistic corrections need to be applied, e.g. ω is replaced by $\omega + \dot{\omega}t$. The measurement of the *Post-Keplerian* (PK) *parameters* such as $\dot{\omega}$ allows a comparison with values expected in the framework of specific theories of gravity.

When a timing model including these parameters is fitted successfully, post-fit residuals expressed in pulse phase show a random distribution around zero. Incorrect or incomplete timing models cause systematic structures in the post-fit residuals identifying the parameter that needs to be included or adjusted (see Fig. 7). The precision of the parameters improves with length of the data span and the frequency of observation, but also with orbital coverage in the case of binary pulsars. Sufficient data sets then enable measurements with amazing precision, e.g. the period determined for PSR B1937+21 is $P = 0.00155780647244881 7 \pm 0.000000000000000003$ s (MJD 47899.5).

8 Pulsars as Tools

Pulsars are unique and versatile objects which can be used to study an extremely wide range of physical and astrophysical problems. Besides testing theories of gravity one can study the Galaxy and the interstellar medium, stars, binary systems and their evolution, solid state physics and the interior of neutron stars. Investigating the radio emission of pulsars provides insight into plasma physics under extreme conditions. The most famous applications of pulsars is their use as clocks and their role in the tests of theories of gravity.

8.1 Pulsars as Clocks

In tests of general relativity and alternative theories, pulsars can be used to study possible violations of the Strong-Equivalence-Principle (SEP), the possible existence of preferred frames or the violation of conversation laws. While these effects

can also be studied in the solar system to some degree, pulsars take us beyond the weak-field limit of the solar-system. Thereby, their contribution is crucial as no test can be considered to be complete without probing the strong-field realm that is only accessible with pulsars. Recent reviews are given by Will (2001), Wex (2000, 2001), Stairs (2003) and Kramer (2004a).

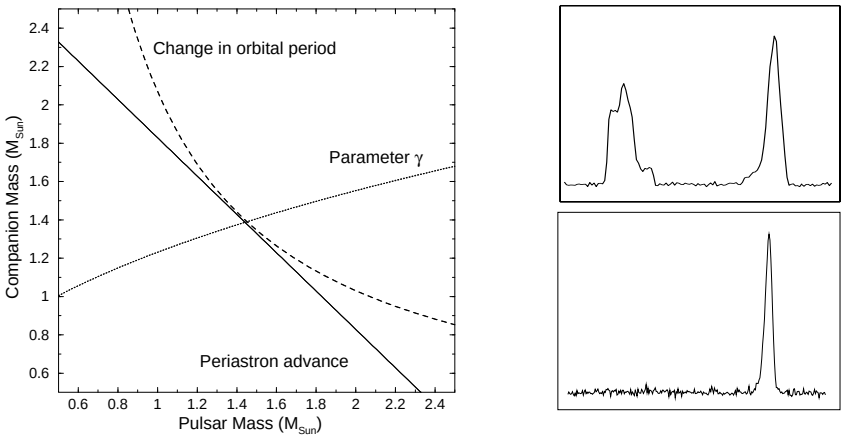

Fig. 8. *Left:* Mass-mass diagram for the DNS PSR B1913+16 using parameters determined by Weisberg & Taylor (2003). The lines as given by general relativity and with line widths that are larger than the corresponding uncertainties all intersect in a single point. *Right:* Pulse profiles of the new DNSs PSR J0737−3039 (top) and J1756−2256 (bottom). These systems promise to provide similar or even better tests than PSR B1913+16.

General relativity has to date passed all observational tests with flying colours. Some of the most stringent tests are provided by double-neutron star systems (DNSs). Because of the strong gravitational fields, we expect DNSs to suffer large relativistic effects. In this case, we cannot necessarily assume that we understand the underlying physics, even though general relativity appears to describe the physics in the solar system to high precision. Therefore, one can only use an existing theory of gravity and check if the observations are consistently described by the measured Keplerian and PK parameters. In each theory, the PK parameters should only be functions of the a priori unknown pulsar and companion mass, M_p and M_c, and the easily measurable Keplerian parameters. With the two masses as the only free parameters during the test, an observation of two PK parameters will already determine the masses uniquely in the framework of the given theory. The measurement of a third or more PK parameters then provides a consistency check. In general relativity, the five most important PK parameters are given by (e.g. Wex 2001):

$$\dot{\omega} \;=\; 3T_{\odot}^{2/3}\left(\frac{P_b}{2\pi}\right)^{-5/3}\frac{1}{1-e^2}\,(M_p+M_c)^{2/3}, \qquad (8.1)$$

$$\gamma = T_\odot^{2/3} \left(\frac{P_b}{2\pi}\right)^{1/3} e \frac{M_c(M_p + 2M_c)}{(M_p + M_c)^{4/3}} \tag{8.2}$$

$$\dot{P}_b = -\frac{192\pi}{5} T_\odot^{5/3} \left(\frac{P_b}{2\pi}\right)^{-5/3} \frac{\left(1 + \frac{73}{24}e^2 + \frac{37}{96}e^4\right)}{(1-e^2)^{7/2}} \frac{M_p M_c}{(M_p + M_c)^{1/3}}, \tag{8.3}$$

$$r = T_\odot M_c, \tag{8.4}$$

$$s = T_\odot^{-1/3} \left(\frac{P_b}{2\pi}\right)^{-2/3} x \frac{(M_p + 2M_c)^{2/3}}{M_c} \tag{8.5}$$

where P_b is the period and e the eccentricity of the binary orbit. The masses M_p and M_c of pulsar and companion, respectively, are expressed in solar masses ($M_\odot$). We define the constant $T_\odot = GM_\odot/c^3 = 4.925490947\mu$s where G denotes the Newtonian constant of gravity and c the speed of light. The first PK parameter, $\dot{\omega}$, is the easiest to measure and describes the relativistic advance of periastron. It provides an immediate measurement of the total mass of the system, $(M_p + M_c)$. The parameter γ denotes the amplitude of delays in arrival times caused by the varying effects of the gravitational redshift and time dilation (second order Doppler) as the pulsar moves in its elliptical orbit at varying distances from the companion and with varying speeds. The decay of the orbit due to gravitational wave damping is expressed by the change in orbital period, $\dot{P}_b$. The other two parameters, r and s, are related to the Shapiro delay caused by the gravitational field of the companion. These parameters are only measurable, depending on timing precision, if the orbit is seen nearly edge-on.

Currently, only two DNSs have more than two PK parameters determined, the 59-ms pulsar B1913+16 and the 38-ms PSR B1534+12. For PSR B1913+16 with an eccentric ($e = 0.61$) 7.8-hr orbit, the PK parameters $\dot{\omega}$, γ and $\dot{P}_b$ are measured very precisely. Correcting the observed $\dot{P}_b$ value for the Shlovskii effect, the measured value is in excellent agreement with the prediction of general relativity for quadrupole emission. The dependencies of the PK parameters on the unknown pulsar and companion masses can be displayed in a M_p-M_c diagram where all lines meet in a single point (0.25% agreement, see Fig. 8). It demonstrates impressively that general relativity provides a self-consistent and accurate description of the system which can be described as orbiting point masses, i.e. the structure of the neutron stars does not influence their orbital motion as expected from SEP. The precision of this test is limited by our knowledge of the Galactic gravitational potential and the corresponding correction to $\dot{P}_b$. The timing results for PSR B1913+16 provide us with the most precise measurements of neutron star masses ever, i.e. $M_p = (1.4408 \pm 0.0003)M_\odot$ and $M_c = (1.3873 \pm 0.0003)M_\odot$ 2003. It is worth pointing out that these values include the unknown Doppler factor.

The 10-hr orbit of the second DNS PSR B1534+14 ($e = 0.27$) is observed under fortunate circumstances, it is seen nearly edge-on. Thereby, in addition to the three PK parameters observed for PSR B1913+16, the Shapiro-delay parameters r and s can be measured, enabling non-radiative aspects of gravitational theories to be tested, as $\dot{P}_b$ is not necessarily needed. In fact, the observed value of $\dot{P}_b$ seems to be heavily influenced by Shlovskii-terms, so that the corresponding line fails to

meet the others in a M_p-M_c diagram. However, assuming that general relativity is the correct theory of gravitation, the deviation from the predicted value and the measured proper motion, μ, can be used to compute the necessary correction and hence the distance to the pulsar, $d = 1.02 \pm 0.05$ kpc (Stairs et al. 2002).

8.2 Tests of Gravity Using Profile Structure Data

In addition to the use of pulsars as clocks, strong gravity effects can also be tested using pulse structure data, namely the effects of "geodetic precession" in the DNSs PSR B1913+16 and PSR B1534+14. In both cases, the pulsar spin axis appears to be misaligned with the orbital angular momentum vector. In such a case, general relativity predicts a relativistic spin-orbit coupling, analogous to spin-orbit coupling in atomic physics. The pulsar spin precesses about the total angular momentum, changing the relative orientation of the pulsar towards Earth. As a result, the angle between the pulsar spin axis and our line-of-sight changes with time, so that different portions of the emission beam are observed (Damour & Ruffini 1974). Consequently, changes in the measured pulse profile and its polarization are expected. In extreme cases, the precession may even move the beam out of our line-of-sight and the pulsar may disappear as predicted for PSR B1913+16 (Kramer 1998). See Kramer (2002) for a detailed review.

9 Pulsars in the Future

The tremendous success of recent surveys using the Parkes telescope (e.g. Manchester 2001) has lead not only to the discovery of more than 700 new pulsars, but also to some very exciting new binary systems. Until recently, only five DNSs were known. This situation has changed and now seven systems can be studied. PSR J0737-3039 was discovered in April 2003 (Burgay et al. 2003, see Fig. 8). The present observations already indicate that it is the most extreme relativistic binary system discovered so far: its short orbital period ($P_b = 2.4$ hrs) together with a remarkable high value of periastron advance ($\dot{\omega} = 16.88 \pm 0.09$ deg/yr, i.e. four times larger than for PSR B1913+16!) and the short coalescing time ($\sim$ 85 Myr) make this system the most beautiful laboratory for testing general relativity found so far. Its discovery shows that the new gravitational wave detectors that are coming on-line, have a much higher chance to detect an event of coalescing neutron stars than previously estimated. Moreover, with a geodetic precession period of only 70 yr future studies of PSR J0737−3039 should reveal interesting profile changes with implications for the pulsar geometry.

These latest results show that the discovery of many new pulsars will eventually also lead to the discovery of very exciting systems. Hence, a telescope with a sensitivity that is high enough to essentially detect every pulsar in the Galaxy must provide us with unique discoveries. Such telescope is planned with the *Square-Kilometre-Array* (SKA). Through its sensitivity, sky and frequency coverage, the SKA will discover – besides extragalactic pulsars – about 10,000 to 20,000 pulsars in the Milky Way, including the discovery of more than 1,000 millisecond pulsars.

In addition to probing the equation-of-state at extreme limits, this impressive yield also effectively samples every possible outcome of the evolution of massive binary stars. We expect at least 100 compact relativistic binaries, providing amazing test grounds for gravitational physics. Finally, the SKA should provide us with "the holy grail" of pulsar-stellar black hole (PSR-BH) systems.

High precision timing observations of a pulsar orbiting a black hole provides tests of relativistic gravity with a discriminating power that surpasses all its present and foreseeable competitors (Damour & Esposito-Farèse 1998). One can not only study stellar black holes but also apply the same timing techniques to pulsars around the super-massive black hole in the Galactic Centre. This allows a direct comparison of the properties of these objects: one can determine mass, spin and quadrupole moment of black holes to test their description in Einstein's theory (the "no-hair"-theorem) for the first time! In addition, the discovered dense array of millisecond pulsars across the sky can be used as multiple arms of a cosmic gravitational wave detector. This "device", with the SKA at its heart, will be sensitive to gravitational waves (GWs) at frequencies of nHz, thereby complementing the much higher frequencies accessible to Advanced LIGO (∼100Hz) and LISA (∼mHz). It can then be used to study the existence, nature and composition of a GW background which is expected from a variety of sources such as coalescence of massive black hole binaries during galaxy evolution or the evolution and decay of cosmic strings as predicted in grand unified theories (see Kramer 2003 for a recent review).

10 Conclusions

While it was immediately realized after the discovery of pulsars more than 35 years ago, that pulsars are unique objects for the study of fundamental physics, it is fair to say that pulsars have exceeded all initial expectations. Still, we have not yet fully explored all opportunities that they provide. This will be possible with the SKA which, as for other areas in modern astronomy, will revolutionize the field of pulsar astrophysics. Not only will new science be possible by the shear number of pulsars discovered, but also by the unique timing precision achievable with the SKA. The combination of both will not simply mean a continuation of the successes already achieved by using pulsars as fundamental tools of physics but the SKA will provide a new quality of science.

References

Alpar, M. A., Cheng, A. F., Ruderman, M. A., and Shaham, J.: 1982, *Nature* **300**, 728

Backer, D. C.: 1995, *J. Astrophys. Astr.* **16**, 165

Backer, D. C., Kulkarni, S. R., Heiles, C., Davis, M. M., and Goss, W. M.: 1982, *Nature* **300**, 615

Baring, M. G. and Harding, A. K.: 1998, *ApJ* **507**, L55

Becker, W. and Aschenbach, B.: 2002, in Becker, W., Lesch, H. and Trümper (eds.), *Neutron Stars, Pulsars, and Supernova Remnants*, MPE-Report 278, pp 64–+

Bignami, G. F., Caraveo, P. A., Luca, A. D., and Mereghetti, S.: 2003, *Nature* **423**, 725

Burgay, M., D'Amico, N., Possenti, A., Manchester, R., Lyne, A. G., Joshi, B. C., McLaughlin, M., Kramer, M., Sarkissian, J. M., and Camilo, F.: 2003, *Nature*, in press

Cheng, K. S., Ho, C., and Ruderman, M.: 1986, *ApJ* **300**, 500

Cognard, I., Shrauner, J. A., Taylor, J. H., and Thorsett, S. E.: 1996, *ApJ* **457**, 81

Cordes, J. M.: 1978, *ApJ* **222**, 1006

Cusumano, G., Hermsen, W., Kramer, M., Kuiper, L., Löhmer, O., Massaro, E., Mineo, T., Nicastro, L., and Stappers, B. W.: 2003, *A&A* **410**, L9

Damour, T. and Esposito-Farèse, G.: 1998, *Phys. Rev. D* **58**, 042001

Damour, T. and Ruffini, R.: 1974, *Academie des Sciences Paris Comptes Rendus Ser. Scie. Math.* **279**, 971

Daugherty, J. K. and Harding, A. K.: 1996, *ApJ* **458**, 278

Deshpande, A. A. and Rankin, J. M.: 2001, *MNRAS* **322**, 438

Gotthelf, E. V., Vasisht, G., Boylan-Kolchin, M., and Torii, K.: 2000, *ApJ* **542**, L37, PSR J1846-0258

Hankins, T. H., Kern, J. S., Weatherall, J. C., and Eilek, J. A.: 2003, *Nature* **422**, 141

Hewish, A., Bell, S. J., Pilkington, J. D. H., Scott, P. F., and Collins, R. A.: 1968, *Nature* **217**, 709

Hobbs, G., Lyne, A. G., Kramer, M., Martin, C. E., and Jordan, C.: 2003, *MNRAS*, submitted

Johnston, S. and Galloway, D.: 1999, *MNRAS* **306**, L50

Johnston, S. and Romani, R. W.: 2003, *ApJ* **590**, L95

Johnston, S., van Straten, W., Kramer, M., and Bailes, M.: 2001, *ApJ* **549**, L101

Joshi, B., Kramer, M., Lyne, A., McLaughlin, M., and Stairs, I.: 2004, in F. Camilo and B. Gaensler (eds.), *Young Neutron Stars and Their Environments (IAU Symposium 218)*, PASP, in press

Kanbach, G.: 2002, in Becker, W., Lesch, H. and Trümper (eds.), *Neutron Stars, Pulsars, and Supernova Remnants*, MPE-Report 278, pp 91–+

Kanbach, G., Kellner, S., Schrey, F. Z., Steinle, H., Straubmeier, C., and Spruit, H. C.: 2003, in *Instrument Design and Performance for Optical/Infrared Ground-based Telescopes. Edited by Iye, Masanori; Moorwood, Alan F. M. Proceedings of the SPIE, Volume 4841, pp. 82-93 (2003).*, pp 82–93

Karastergiou, A., Johnston, S., and Kramer, M.: 2003, *A&A* **404**, 325

Karastergiou, A., Johnston, S., Kramer, M., Bhat, N., and Gupta, Y.: 2004, in F. Camilo and B. Gaensler (eds.), *Young Neutron Stars and Their Environments (IAU Symposium 218)*, PASP, in press

Karastergiou, A., Kramer, M., Johnston, S., Lyne, A. G., Bhat, N. D. R., and Gupta, Y.: 2002, *A&A* **391**, 247

Karastergiou, A., von Hoensbroech, A., Kramer, M., Lorimer, D., Lyne, A., Doroshenko, O., Jessner, A., Jordan, A., and Wielebinski, R.: 2001, *A&A* **379**, 270

Kaspi, V.: 2004, in F. Camilo and B. Gaensler (eds.), *Young Neutron Stars and Their Environments (IAU Symposium 218)*, PASP, in press

Kaspi, V. M., Lyne, A. G., Manchester, R. N., Crawford, F., Camilo, F., Bell, J. F., D'Amico, N., Stairs, I. H., McKay, N. P. F., Morris, D. J., and Possenti, A.: 2000, *ApJ* **543**, 321

Kramer, M.: 1998, *ApJ* **509**, 856

Kramer, M.: 2002, in Gurzadyan, V.G. and Jantzen, R.T. and Ruffini, R. (eds.), *The Ninth Marcel Grossmann Meeting*, World Scientific (Singapore), pp 219–+

Kramer, M.: 2003, in Kramer, M. and Rawlings, S. (eds.), *UK SKA-Workshop*, (astro-ph/0306456)

Kramer, M.: 2004a, in S. Karshenboim and E. Peik (eds.), *Astrophysics, Clocks, and Fundamental Constants*, Springer, in press

Kramer, M.: 2004b, in F. Camilo and B. Gaensler (eds.), *Young Neutron Stars and Their Environments (IAU Symposium 218)*, PASP, in press (astro-ph/0310451)

Kramer, M., Bell, J. F., Manchester, R. N., Lyne, A. G., Camilo, F., Stairs, I. H., D'Amico, N., Kaspi, V. M., Hobbs, G., Morris, D. J., Crawford, F., Possenti, A., Joshi, B. C., McLaughlin, M. A., Lorimer, D. R., and Faulkner, A. J.: 2003a, *MNRAS* **342**, 1299

Kramer, M., Karastergiou, A., Gupta, Y., Johnston, S., Bhat, N. D. R., and Lyne, A. G.: 2003b, *A&A* **407**, 655

Kramer, M., Lyne, A. G., Hobbs, G., Löhmer, O., Carr, P., Jordan, C., and Wolszczan, A.: 2003c, *ApJ* **593**, L31

Kramer, M., Xilouris, K. M., Jessner, A., Lorimer, D. R., Wielebinski, R., and Lyne, A. G.: 1997, *A&A* **322**, 846

Kramer, M., Xilouris, K. M., Jessner, A., and Wielebinski, R.; Timofeev, M.: 1996, *A&A* **306**, 867

Kramer, M., Xilouris, K. M., Lorimer, D. R., Doroshenko, O., Jessner, A., Wielebinski, R., Wolszczan, A., and Camilo, F.: 1998, *ApJ* **501**, 270

Lattimer, J. M. and Prakash, M.: 2001, *ApJ* **550**, 426

Link, B., Epstein, R. I. and Lattimer, J. M.: 1999, *Phys. Rev. Lett.* **83**, 3362

Lorimer, D. R. and Xilouris, K. M.: 2000, *ApJ* **545**, 385

Lyne, A. G., Pritchard, R. S., and Smith, F. G.: 1993, *MNRAS* **265**, 1003

Manchester, R. N., Lyne, A. G., Camilo, F., Bell, J. F., Kaspi, V. M., D'Amico, N., McKay, N. P. F., Crawford, F., Stairs, I. H., Possenti, A., Morris, D. J., and Sheppard, D. C.: 2001, *MNRAS* **328**, 17

Maron, O., Kijak, J., Kramer, M., and Wielebinski, R.: 2000, *A&AS* **147**, 195

Marshall, F. E., Gotthelf, E. V., Zhang, W., Middleditch, J., and Wang, Q. D.: 1998, *ApJ* **499**, L179

McLaughlin, M. A., Mattox, J. R., Cordes, J. M., and Thompson, D. J.: 1996, *ApJ* **473**, 763

McLaughlin, M. A., Stairs, I. H., Kaspi, V. M., Lorimer, D. R., Kramer, M., Lyne, A. G., Manchester, R. N., Camilo, F., Hobbs, G., Possenti, A., D'Amico, N., and Faulkner, A. J.: 2003, *ApJ* **591**, L135

Moffett, D. A. and Hankins, T. H.: 1996, *ApJ* **468**, 779

Morris, D., Kramer, M., Thum, C., and et al.: 1997, *A&A* **322**, L17

Nicastro, L., Cusumano, G., Loehmer, O., Kramer, M., Kuiper, L., Hermsen, W., Mineo, T., and Becker, W.: 2003, *A&A*, in press (astro-ph/0310299)

Oppenheimer, J. R. and Volkoff, G.: 1939, *Phys. Rev.* **55**, 374

Radhakrishnan, V. and Cooke, D. J.: 1969, *Astrophys. Lett.* **3**, 225

Romani, R. and Johnston, S.: 2001, *ApJ* **557**, L93

Romani, R. W., Miller, A. J., Cabrera, B., Nam, S. W. and Martinis, J. M.: 2001, *ApJ* **563**, 221

Sallmen, S., Backer, D. C., Hankins, T. H., Moffett, D., and Lundgren, S.: 1999, *ApJ* **517**, 460

Shapiro, I. I.: 1964, *Phys. Rev. Lett.* **13**, 789

Shearer, A. and Golden, A.: 2002, in Becker, W., Lesch, H. and Trümper (eds.), *Neutron Stars, Pulsars, and Supernova Remnants*, MPE-Report 278, pp 44–+

Shearer, A., Stappers, B., O'Connor, P., Golden, A., Strom, R., Redfern, M., and Ryan, O.: 2003, *Science* **301**, 493

Staelin, D. H. and Reifenstein, III, E. C.: 1968, *Science* **162**, 1481

Stairs, I. H.: 2003, *Living Rev. Relativity* 6, 5. [Online article]: cited on 1 Oct 2003, http://www.livingreviews.org/lrr-2003-5

Stairs, I. H., Thorsett, S. E., Taylor, J. H., and Wolszczan, A.: 2002, *ApJ* **581**, 501

Thompson, D. J.: 2001, in *High Energy Gamma-Ray Astronomy*, pp 103–+

Thorsett, S. E. and Chakrabarty, D.: 1999, *ApJ* **512**, 288

Weisberg, J. M. and Taylor, J. H.: 2003, in *Radio Pulsars, ASP Conf. Series Vol. 302*, pp 93–98, PASP, San Francisco

Wex, N.: 2000, in M. Kramer, N. Wex, and R. Wielebinski (eds.), *Pulsar Astronomy - 2000 and Beyond, IAU Colloquium 177*, pp 113–116, Astronomical Society of the Pacific, San Francisco

Wex, N.: 2001, in C. Lämmerzahl and F. W. Everitt, C. W. F. Hehl (eds.), *Gyros, Clocks, Interferometers...: Testing Relativistic Gravity in Space*, Springer

Will, C. M.: 2001, *Living Rev. Relativity* 4, 4. [Online article]: cited on 1 Oct 2003, http://www.livingreviews.org/lrr-2001-4

Xilouris, K. M., Kramer, M., Jessner, A., Wielebinski, R., and Timofeev, M.: 1996, *A&A* **309**, 481

Young, M. D., Manchester, R. N., and Johnston, S.: 1999, *Nature* **400**, 848

Zavlin, V. E. and Pavlov, G. G.: 1998, *A&A* **329**, 583

Zhang, B. and Harding, A. K.: 2000, *ApJ* **535**, L51

Zhang, W., Marshall, F. E., Gotthelf, E. V., Middleditch, J., and Wang, Q. D.: 2001, *ApJ* **554**, L177